Digest Journal of Nanomaterials and Biostructures Vol. 19, No. 4, October-December 2024, p. 1711-1718

Preparation of g-C_3N_4 nanosheets for enhanced removal of tetracycline

J. L. Guo [a], Y. Q. Dong [a], Y. H. Ding [a], S. J. Hu [a], H. R. Dong [a], S. M. Lv [a], K. Lei [a], Y. J. Duan [a], X. H. Zeng [a], Wei Feng [a,b], Y. Sun [a,*]
[a] *School of Mechanical Engineering, Chengdu University, Chengdu, 610106, China*
[b] *Material Corrosion and Protection Key Laboratory of Sichuan province, Zigong, 643002, China*

Two-dimensional (2D) structure g-C_3N_4 was prepared via thermal oxidation etching at different temperatures. Under simulated solar illumination, the photocatalytic properties of catalysts were estimated by degrading tetracycline (TC). Owing to the enlarged specific surface area, 2D g-C_3N_4 nanosheets demonstrated superior photocatalytic performance. Furthermore, as the temperature increased, the degradation efficiency also increased. When bulk g-C_3N_4 was exfoliated at 525°C, the highest degradation efficiency of TC reached 84.0%.

(Received September 11, 2024; Accepted November 9, 2024)

Keywords: g-C_3N_4 nanosheets, Thermal oxidation etching, Photocatalytic degradation, Tetracycline

1. Introduction

To date, due to the overuse of antibiotics and discharge of wastewater, residual antibiotics have entered the natural environment, which is harmful to human health and ecological environment [1]. So far, various treatment technologies have been introduced to process the antibiotic industrial wastewater, including physical adsorption [2], biodegradation [3], photocatalysis [4]. Among these methods, semiconductor photocatalysis is a promising approach for utilizing renewable solar energy to decompose and mineralize organic pollutants. Owing to the distinctive layered structure, adjustable bandgap, metal-free properties, and excellent physicochemical stability [5-8], g-C_3N_4 has garnered much interest in the field of photocatalysis. Nevertheless, the practical implementation is restricted by the fast recombination of photoinduced electrons-holes, less active sites, and low quantum efficiency [9]. Currently, numerous strategies have been studied to boost photocatalytic properties of g-C_3N_4 through morphology control [10], element doping [11], and heterostructure construction [12].

2D g-C_3N_4 nanosheets, as efficient catalysts with higher surface area, can offer abundant active sites for photocatalytic reactions [13]. Thermal etching of g-C_3N_4 in air is a low-cost and environmentally friendly way to synthesize g-C_3N_4 nanosheets [14-19]. Li et al. [20] reported exfoliated g-C_3N_4 with various nanostructures was achieved through adjustments in exfoliation temperature and time. As the temperature increased from 500°C to 550°C, bulk g-C_3N_4 was oxidized layer by layer, and foamy g-C_3N_4 was formed after 6 h. Wu et al. [21] fabricated g-C_3N_4 nanosheets through repeatedly calcination of pristine g-C_3N_4 at 600°C, demonstrating excellent removal efficiency of nitric oxide. Thus, this thermal oxidation etching process is recognized as an effective and simple way to improve photocatalytic properties of g-C_3N_4 [22].

In this research, 2D g-C3N4 were synthesized via thermal etching at different temperatures. Photocatalytic properties of catalysts were assessed by degradation of tetracycline. Furthermore, photocatalytic degradation mechanism was discussed by identifying active species.

* Corresponding author: sunyan@cdu.edu.cn
https://doi.org/10.15251/DJNB.2024.194.1711

2. Experimental

2.1. Preparation

Pristine g-C_3N_4 was prepared through thermal polymerization process [23]. 5.0 g of melamine was heated in air at 550°C for 4 hours. After calcination, the resulting yellowish powder was obtained and named as CN.

1.0 g of CN was calcined in an open ceramic crucible with different temperatures (400°C, 425°C, 450°C, 475°C, 500°C, and 525°C) at 5°C/min for 2 h. The samples were marked as 400-CN, 425-CN, 450-CN, 475-CN, 500-CN, and 525-CN, respectively.

2.2. Characterization

Crystalline structure was detected by X-ray diffraction (XRD, DX-2700B). Morphology and microstructure were examined using scanning electron microscopy (SEM, ZEISS Sigma 300) and transmission electron microscopy (TEM, Talos F200S). Surface composition and valence band are obtained using X-ray photoelectron spectroscopy (XPS, Escalab Xi+). The TU-1901 spectrometer was used to analyze the optical properties. V-Sorb 2800P surface area analyzer was employed to determine the Brunauer-Emmet-Teller (BET) surface area.

2.3. Photocatalytic properties

Photocatalytic removal of TC was conducted using a 500 W Xenon lamp. 0.04 g of catalyst powder was put to 100 mL of TC solution (20 mg/L) with continuous stirring. After irradiation, the concentration of TC was obtained via a UV-vis spectrophotometer.

3. Results and discussion

Fig 1 displays XRD patterns of all samples. Two peaks at 13.1° (100) and 27.3° (002) are indexed to in-plane structural mode and interlayer stacking [24], respectively. As g-C_3N_4 was exfoliated from 400°C to 525°C, a small shift of (002) plane peak to a higher angle appears, indicating a gradual reduction in the layer spacing.

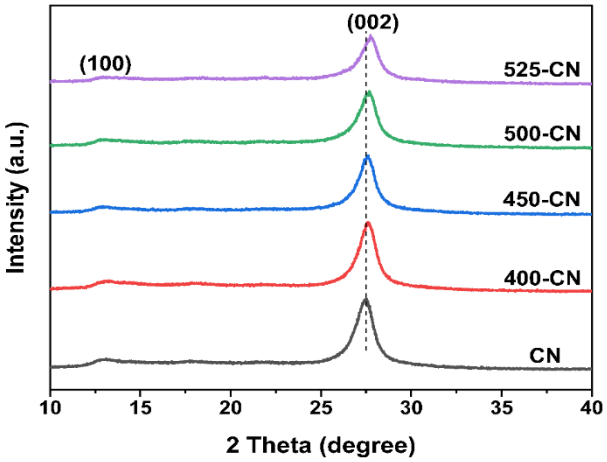

Fig. 1. XRD patterns of various catalysts.

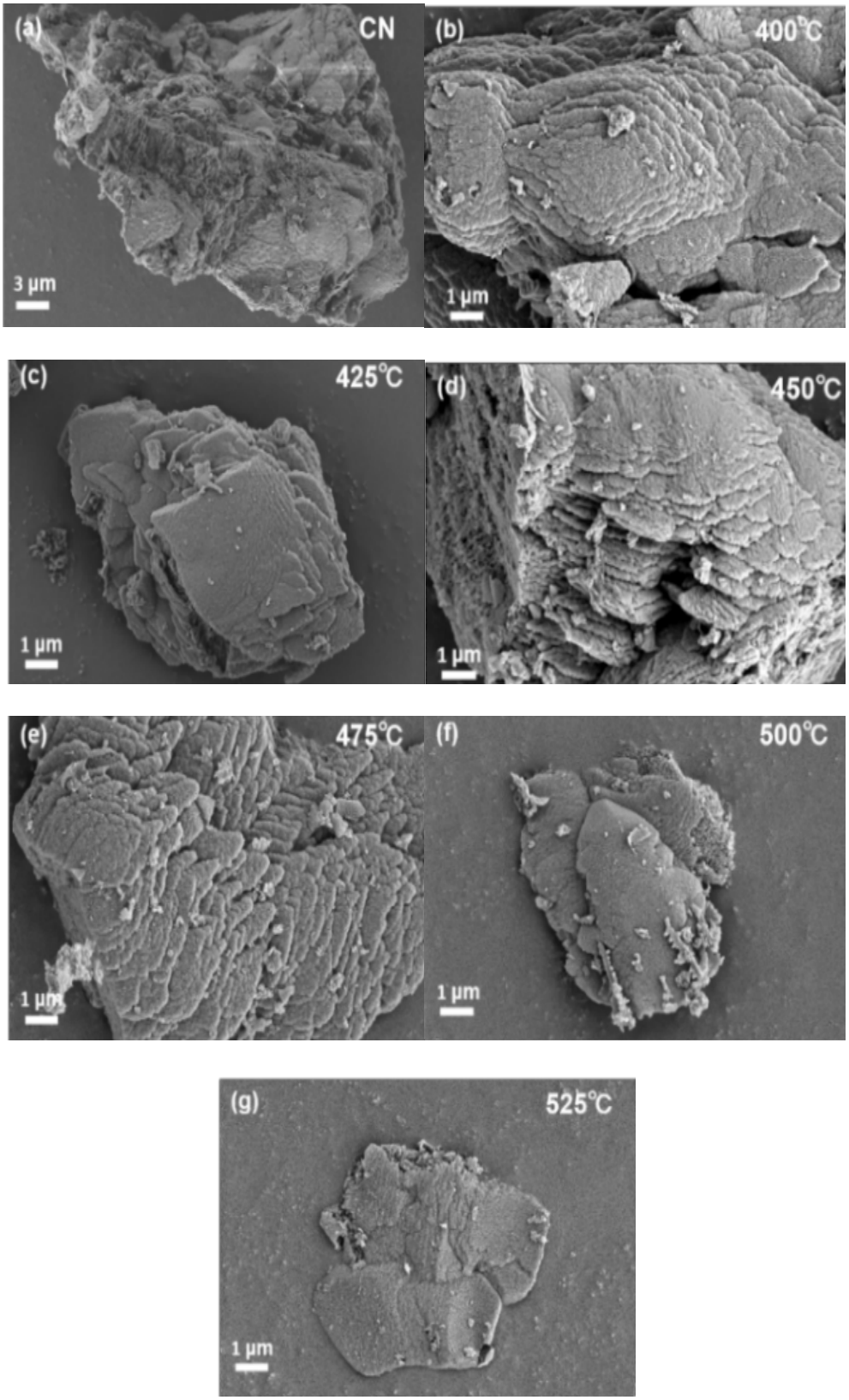

Fig. 2. SEM images of synthesized samples: (a) CN, (b) 400-CN, (c) 425-CN, (d) 450-CN, (e) 475-CN, (f) 500-CN and (g) 525-CN.

Fig 2a is SEM image of bulk g-C_3N_4 with characteristic layered stacked structure. Fig 2b-e illustrate that as the thermal etching temperature of CN increases from 400°C to 475°C, the particle size of g-C_3N_4 becomes smaller the thickness becomes thinner. At higher calcination temperatures of 500°C and 525°C (Fig 2f-g), bulk g-C_3N_4 has completely been stripped to nanosheets. The increasing thermal etching temperature breaks van der Waals forces between layers, leading to improvement of specific surface area.

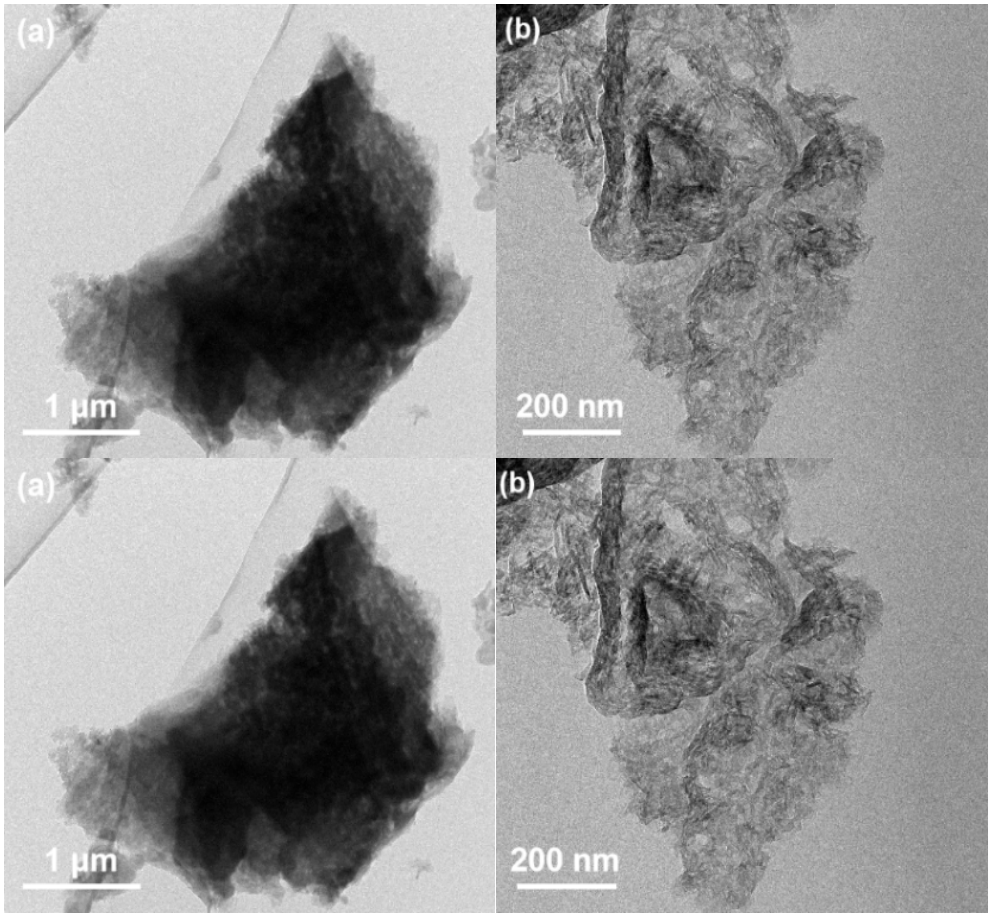

Fig. 3. TEM images of (a) CN and (b) 525-CN.

TEM images of CN and 525-CN samples are shown in Fig 3. Compared with CN, 525-CN exhibits an ultrathin 2D sheet-like structure and the thickness is much smaller. The results further verify that CN could be exfoliated into 2D g-C_3N_4 via the thermal etching process.

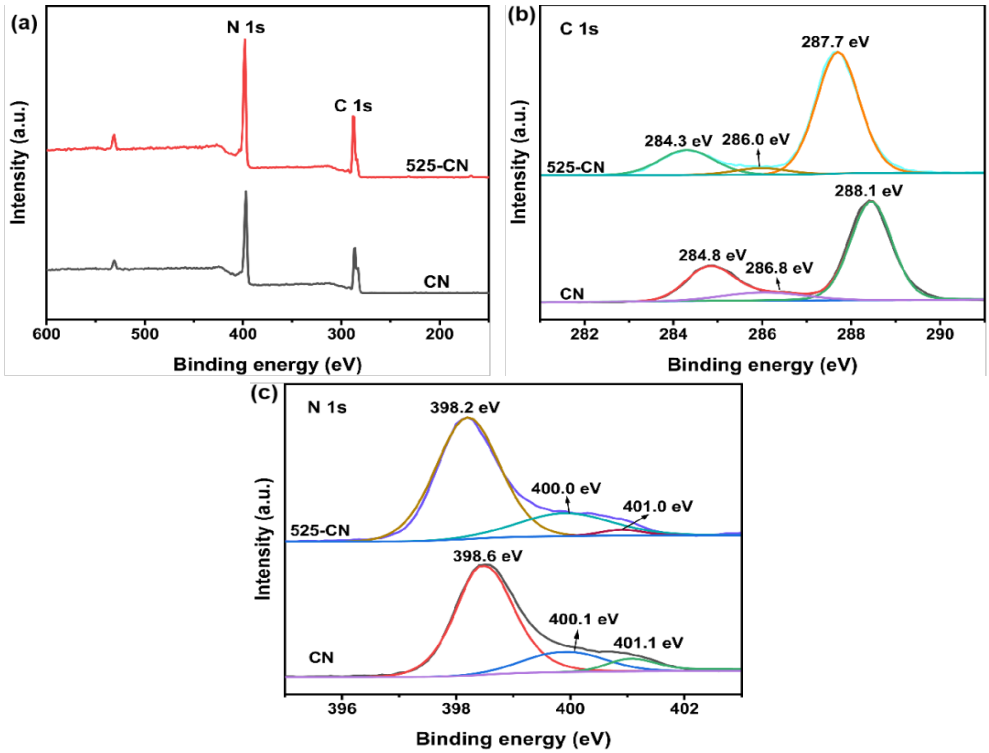

Fig. 4. XPS spectra: (a) survey, (b) C 1s and (c) N 1s.

The survey spectra (Fig. 4a) of CN and 525-CN samples indicates the samples contain C and N elements. In C 1s spectra (Fig. 4b), three peaks of CN sample at 284.8, 286.8, and 288.1 eV belong to C-C, C-N, and N-C=N bonds, respectively. The N 1s spectrum of CN (Fig. 4c) displays three peaks at 398.6, 400.1, and 401.1 eV, corresponding to C-N=C, N–$(C)_3$, and N–H bonds, respectively [25]. Notably, both C1s and N1s peaks of 525-CN sample shift toward the lower binding energies, which are attributed to the inter laminar peeling effect.

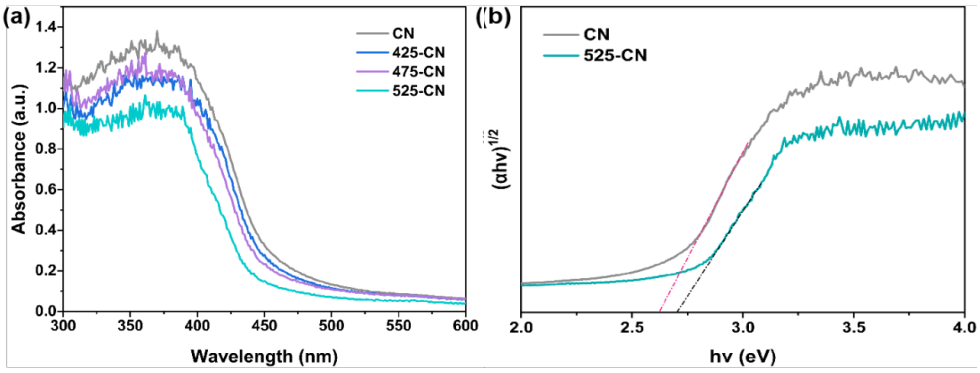

Fig. 5. (a) UV-vis diffuse reflectance spectra; (b) bandgap of CN and 525-CN.

Fig. 5a shows optical properties of CN and 2D g-C_3N_4 calcined at various temperatures. CN exhibits an absorption edge at 463 nm while the light absorption edge of 2D g-C_3N_4 samples show an obvious blue shift owing to the quantum confinement effect. Using Tauc plot function equation $\alpha hv=A(hv-E_g)^{n/2}$ [26], the bandgap of CN and 525-CN is determined as 2.57 eV and 2.70 eV.

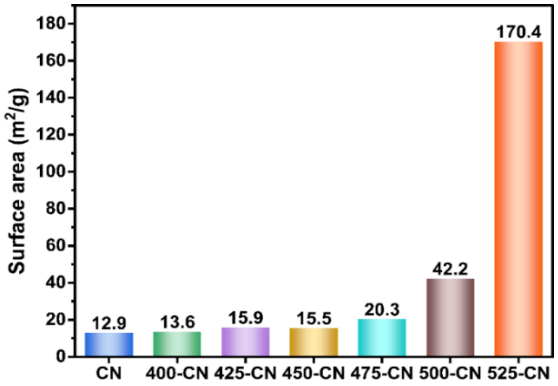

Fig. 6. Comparison of specific surface area.

Fig 6 compares the surface area of prepared catalysts. The surface areas of CN, 400-CN，425-CN, 450-CN, 475-CN, 500-CN and 525-CN samples are 12.9, 13.6, 15.9, 15.5, 20.3, 42.2 and 170.4 m^2/g, respectively. The enhancement in surface area with increasing in etching temperature is ascribed to the gradual stripping of the sample into the nanosheets structure.

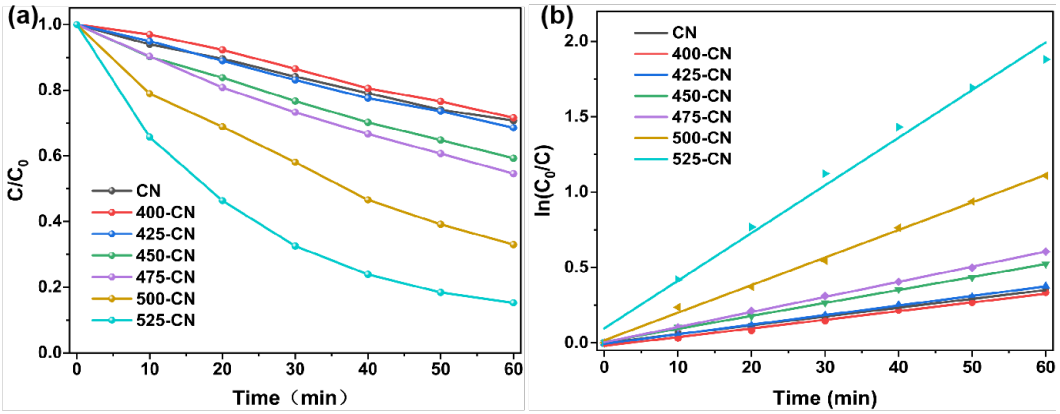

Fig. 7. TC degradation (a) and corresponding first-order kinetics curves (b).

Fig 7a compares the photocatalytic degradation efficiency of different catalysts. For CN sample, only 29.1% of TC can be decomposed within 60 min. After thermal etching at 400°C, the TC degradation efficiency is close to that of CN sample. Particularly, the degradation efficiency increases with the increase of etching temperature and the degradation efficiency of 425-CN, 450-CN, 475-CN, 500-CN and 525-CN is 31.4%, 40.7%, 45.4%, 67.0% and 84.0%, respectively. As the surface area of the catalysts increase with thermal etching temperature, more active sites can involve in the photocatalytic reaction, consequently enhancing the degradation efficiency. The reaction kinetics of TC degradation (Fig 7b) shows good linearity, meaning that the TC degradation of all catalysts follows first-order reaction kinetics. The reaction rate of CN, 400-CN, 425-CN, 450-CN, 475-CN, 500-CN, and 525-CN is 0.00585, 0.00575, 0.00635, 0.0086, 0.01225, 0.01829, and 0.0297min^{-1}, respectively. The reaction rate of 525-CN is 5.08 times that of CN.

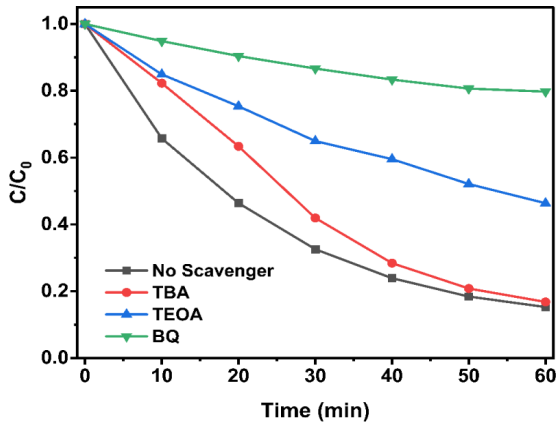

Fig. 8. The effect of scavenger on the TC degradation of 525-CN.

Capture experiments were conducted to explore active species involved in photocatalytic reaction. 1 mM of 1,4-benzoquinone (BQ), 10 mM of Tertiary-butyl alcohol (TBA), and 15 mM of triethanolamine (TEOA) were employed to capture $\cdot O_2^-$, $\cdot OH$, and h^+, respectively. As demonstrated in Fig 8, after adding TBA, the degradation efficiency has no great change, indicating that $\cdot OH$ hardly participates in the degradation of TC. However, the TC degradation efficiency significantly decline to 20.3%, and 53.2% as a result of the introduction of BQ and TEOA, respectively, which means the primary active species are $\cdot O_2^-$ and h^+ during the degradation.

4. Conclusion

In summary, 2D structure g-C_3N_4 was fabricated through thermal etching by varying etching temperature. The surface area of g-C_3N_4 nanosheets significantly increased with increasing temperature. Followed by exfoliation of bulk g-C_3N_4 at 525°C, 2D structure g-C_3N_4 exhibited a significant enhancement in the specific surface area, reaching 170.4 m^2/g. Consequently, the photocatalytic degradation of tetracycline achieved the maximum of 84.0% within 60 minutes. Furthermore, the trapping experiment results revealed that $\cdot O_2^-$ and h^+ played crucial roles during TC degradation process. This work was supported by the Opening Project of Material Corrosion and Protection Key Laboratory of Sichuan province (No.2023CL01).

Acknowledgments

This work was supported by the Opening Project of Material Corrosion and Protection Key Laboratory of Sichuan province (No.2023CL01).

References

[1] T. Yu, B. Yang, R. Zhang, C. Yang, J. Jiang, Journal of Materials Science & Technology, 188, 11-26 (2024); https://doi.org/10.1016/j.jmst.2023.12.004

[2] X. Huang, W. Mu, C. Chang, Journal of Alloys and Compounds, 968, 172012 (2023); https://doi.org/10.1016/j.jallcom.2023.172012

[3] M. B. Ahmed, J. L. Zhou, H. H. Ngo, W. Guo, N. S Thomaidis, Journal of hazardous materials, 323, 274-298 (2017); https://doi.org/10.1016/j.jhazmat.2016.04.045

[4] S. L. Pu, Y. M. Chen, D.Y. Wang, Y. C. Zhang, Y Li, W Feng, Y Sun, Optical Materials, 141, 113888 (2023); https://doi.org/10.1016/j.optmat.2023.113888

[5] J. Zhang, Y. Zhao, K. Qi, S. Liu, Journal of Materials Science & Technology, 172, 145-155 (2024); https://doi.org/10.1016/j.jmst.2023.06.042

[6] J. Tian, Z. Zhu, B. Liu, Colloids and Surfaces A: Physicochemical and Engineering Aspects, 581, 123798 (2019); https://doi.org/10.1016/j.colsurfa.2019.123798

[7] Y. Yang, G. Li, Z. Li, L. Lu, Science of The Total Environment, 172851(2024); https://doi.org/10.1016/j.scitotenv.2024.172851

[8] C. Hu, H. Huang, Acta Physico Chimica Sinica, 39 (11), 2212048 (2023); https://doi.org/10.3866/PKU.WHXB202212048

[9] X. Liu, R. Ma, L. Zhuang, B. Hu, J. Chen, X. Liu, X. Wang, Critical Reviews in Environmental Science and Technology, 51, 751-790 (2021); https://doi.org/10.1080/10643389.2020.1734433

[10] P. H. Linh, P. D. Chung, N. Van. Khien, V. T. Thu, Diamond and Related Materials, 111, 108214 (2021); https://doi.org/10.1016/j.diamond.2020.108214

[11] Y. Song, Z. Li, S. Li, C. Yang, L. Huang, X. Zhang, Q. Wang, H. Zhan, Journal of Water Process Engineering, 58, 104936 (2024); https://doi.org/10.1016/j.jwpe.2024.104936

[12] Y. M. Dai, W. J. Chen, C. M. Chang, Optical Materials, 148, 1149259 (2024); https://doi.org/10.1016/j.optmat.2024.114925

[13] Y. Wang, L. Liu, T. Ma, Y. Zhang, H. Huang, Advanced Functional Materials, 31 (34), 2102540 (2021); https://doi.org/10.1002/adfm.202102540

[14] Z. H. Jabbar, B. H. Graimed, S. H. Ammar, AA. Najim. Taher, Materials Science in Semiconductor Processing, 173, 108153 (2024); https://doi.org/10.1016/j.mssp.2024.108153

[15] M. Inagaki, T. Tsumura, T. Kinumoto, M. Toyoda, Carbon, 141, 580-607 (2018); https://doi.org/10.1016/j.carbon.2018.09.082

[16] S. Ganesan, T. Kokulnathan, S. Sumathi, A. Palaniappan, Scientific Reports, 14(1), 2284 (2024); https://doi.org/10.1038/s41598-024-52688-y

[17] Q. Qian, D. Kong, S. Zhao, G. Li, X. Cheng, N. Wang, Optics & Laser Technology, 111, 597-603 (2019); https://doi.org/10.1016/j.optlastec.2018.10.041

[18] T. K. A. Nguyen, T. T. Pham, B. Gendensuren, E. S. Oh, E. W. Shin, Journal of Materials Science & Technology, 103, 232-243 (2022); https://doi.org/10.1016/j.jmst.2021.07.013

[19] M. F. Vega, C. Olivas, E. Díaz-Faes, C. Barriocanal, Catalysis Today, 427, 114412 (2024); https://doi.org/10.1016/j.cattod.2023.114412

[20] Y. Li, M. Q. Wang, S. J. Bao, S. Lu, M. Xu, D. Long, S. Pu, Ceramics International, 42 (16), 18521-18528 (2016); https://doi.org/10.1016/j.ceramint.2016.08.190

[21] Wu. X., J. Cheng, X. Li, Y. Li, K. Lv, Applied Surface Science, 465, 1037-1046 (2019); https://doi.org/10.1016/j.apsusc.2018.09.165

[22] M. F. Vega, C. Olivas, E. Díaz-Faes, C. Barriocanal, Catalysis Today, 427, 114412 (2024); https://doi.org/10.1016/j.cattod.2023.114412

[23] X. Luo, Y. Dong, D. Y. Wang, Y. J. Duan, K. Lei, L. Mao, Y. Li, Q. Zhao, Y. Sun, Reviews on Advanced Materials Science, 62(1), 20230123 (2023); https://doi.org/10.1515/rams-2023-0123

[24] Y. Chen, B. Yang, W. Y. Xie, X. Y. Zhao, Z. Wang, X. Su, C. Yang, Journal of Materials Research and Technology, 13, 301-310 (2021); https://doi.org/10.1016/j.jmrt.2021.04.056

[25] M. S. Athar, N. Saleem, I. Ahmad, M. Fzail, T. Ahmad, M. Muneer, Materials Today Sustainability, 26, 100779 (2024); https://doi.org/10.1016/j.mtsust.2024.100779

[26] Y. M. Chen, S. L. Pu, D. Y. Wang, Y. C. Zhang, G. J. Wang, Q. Zhao, Y. Sun, Journal of Solid State Chemistry, 321, 123857 (2023); https://doi.org/10.1016/j.jssc.2023.123857